ResearchGate

See discussions, stats, and author profiles for this publication at: https://www.researchgate.net/publication/268793414

Effect of electrochemical dissolution and deposition order on lithium dendrite formation: A top view investigation

Article in Faraday Discussions · November 2014

DOI: 10.1039/c4fd00124a · Source: PubMed

CITATIONS READS

6 50

12 authors, including:



Xianlong Wei Peking University

69 PUBLICATIONS **1,152** CITATIONS

SEE PROFILE



Qing Chen

Peking University

181 PUBLICATIONS **6,704** CITATIONS

SEE PROFILE

Some of the authors of this publication are also working on these related projects:



Solid state battery View project

Available from: Qing Chen Retrieved on: 24 November 2016



Volume 176

Next-Generation Materials for Energy Chemistry



Faraday Discussions

Cite this: Faraday Discuss., 2014, 176, 109



PAPER

View Article Online
View Journal | View Issue

Effect of electrochemical dissolution and deposition order on lithium dendrite formation: a top view investigation

Wenjun Li,†^a Hao Zheng,†^a Geng Chu,^a Fei Luo,^a Jieyun Zheng,^a Dongdong Xiao,^a Xing Li,^b Lin Gu,*^a Hong Li,*^a Xianlong Wei,^b Qing Chen^b and Liquan Chen^a

Received 4th June 2014, Accepted 14th August 2014

DOI: 10.1039/c4fd00124a

Rechargeable metallic lithium batteries are the ultimate solution to electrochemical storage due to their high theoretical energy densities. One of the key technological challenges is to control the morphology of metallic lithium electrode during electrochemical dissolution and deposition. Here we have investigated the morphology change of metallic lithium electrode after charging and discharging in nonaqueous batteries by ex situ SEM techniques from a top view. Formation of the hole structure after lithium dissolution and the filling of dendrite-like lithium into the holes has been observed for the first time. In addition, an in situ SEM investigation using an all-solid Li/Li₂O/super aligned carbon nanotube set-up indicates that lithium ions could diffuse across through the surface oxide layer and grow lithium dendrites after applying an external electric field. The growth of lithium dendrites can be guided by electron flow when the formed lithium dendrite touches the carbon nanotube.

Introduction

High energy density rechargeable batteries are the key technology to support rapid developments of many emerging technologies, such as advanced portable and wearable electronic devices, electrical vehicles, smart grids, tools and toys, robots, and back-up batteries for various applications. According to thermodynamic calculations, the Li-O₂ battery has the highest theoretical gravimetric energy density among chemical energy storage devices.¹ For similar chemical reactions, batteries with a lithium anode have the highest energy density among other batteries with different metal anodes, such as Mg, Al, Na and Zn. In addition, rechargeable metallic lithium batteries (RMLB) have much higher energy

^aBeijing National Laboratory for Condensed Matter Physics, Institute of Physics, Chinese Academy of Sciences, Beijing, 100190, P. R. China. E-mail: l.gu@iphy.ac.cn; hli@iphy.ac.cn

^bKey Laboratory for the Physics and Chemistry of Nanodevices, Department of Electronics, Peking University, Beijing 100871, P. R. China

[†] Wenjun Li and Hao Zheng contributed equally.

densities than lithium ion batteries (LIB) with the same cathode.¹ Recently, the developing of RMLB has attracted increasing attention after the first wave in the 1970s, especially on Li–S, Li–air, and all solid lithium batteries (ASLB) using polymer or ceramic as electrolytes.²-6 However, periodic dissolution and deposition of metallic lithium during cycling leads to the formation of microstructured or nanostructured lithium with different morphologies, such as needle-like, dendrite, granular and mossy lithium. The newly formed structured lithium reacts significantly with nonaqueous electrolyte electrochemically and chemically.^{7,8} The products are electronically insulating and ionically conducting solid electrolyte interphase (SEI) films. The formation of SEI is unavoidable in nonaqueous lithium batteries, leading to the irreversible consumption of electrolyte and isolation of active lithium. Consequently, the coulombic efficiency of the battery is decreased and the cyclic performance is poor. In addition, structured lithium becomes more dangerous and could cause an internal short circuit, rapid heating and explosion of the battery.⁷⁻⁹

Several strategies have been attempted to control the morphology of metallic lithium electrodes during cycling, including tuning the solvent and salt, ionic liquids, functional additives to modify SEI, suppress lithium dendrites by tuning the local electrical field, lithium surface coating, solid electrolytes, ceramic separators, 3D current collectors, using lithium powder instead of lithium foil, and mechanical pressing.8 In spite of great efforts in improving the performance of metallic lithium electrodes, investigation of the morphology and surface composition are quite challenging due to the soft and air-sensitive nature of the lithium electrode. Ex situ and in situ scanning electronic microscopy (SEM) has been used widely to investigate lithium dendrites in lithium nonaqueous batteries, 10-12 and lithium polymer batteries. 13-15 Atomic force microscopy, 16,17 optical spectroscopy,18 and magnetic resonance imaging (MRI) technology19 have also been used to investigate the morphology change of lithium electrodes. In situ NMR was also developed successfully to quantify the amount of dendritic/mossy Li by analyzing the change in the NMR signal intensity of the Li metal during cycling.20 Fourier transmission infrared spectroscopy (FTIR),11,21,22 X-ray photoelectronic spectroscopy (XPS), 22-24 Raman spectroscopy, 25,26 and secondary ion mass spectroscopy (SIMS)²² have been used to identify the surface composition of reacted lithium electrodes. Electrochemical impedance spectroscopy (EIS) and cyclic voltammetry (CV) have been performed to analyze the electrical response of the lithium electrode.11,16

For the rechargeable lithium battery with a cathode containing the lithium source, such as a Li/LiCoO₂ cell, the deposition of lithium occurs firstly during the first charging then follows the dissolution of lithium during discharging. In the case of rechargeable lithium batteries with a lithium anode as the lithium source, such as Li–S, Li–air batteries, the dissolution of lithium occurs firstly during the first discharge then follows the deposition. There are few reports to distinguish the effect of the order of dissolution and deposition on the morphology of the lithium electrode. In this work, we have investigated the order effect of dissolution and deposition by comparing the morphology change of the metallic lithium electrodes in Li/Si cells, and Li/LiCoO₂ and Li/LiFePO₄ cells respectively. It is obvious that the top view is favorable for the investigation of the morphology change of the lithium electrode. There are very few top-view SEM images of reacted lithium since the lithium electrode is soft and the sample transfer could

change the morphology completely. In order to solve this problem, a special stainless steel sample holder was designed. The soft lithium sheet can be embedded into the hole of the SS substrate and the surface of the lithium can be flattened by mechanical pressing. Transfer of the lithium electrode was performed by contact with the hard edge of the SS sample holder. In addition, our Hitachi SEM instrument has a specially designed sealed sample transfer box, which allows the transfer of the air-sensitive sample from the Ar-filled glove box to the vacuum chamber of the SEM microscope without exposure to air.

Experimental

Flatten lithium sheet for this study

The lithium sheet (4 mm in diameter, 0.45 mm in thickness) in the SS sample holder was pressed by a precisely polished stainless steel pillar to flatten its surface. The roughness of the lithium foil before and after pressing was measured by a MultiMode 8 (BRUKER) scanning probe microscope (SPM) equipped in an Arfilled glove box.²⁷ Atomic force microscope (AFM) images are shown in Fig. 1. The surface roughness is defined by root-mean-squared (RMS) values calculated from the AFM images.²⁷ As shown in Fig. 1 and Table 1, the surface roughness of the pressed lithium foil is much smaller than the unpressed one. Therefore, the pressed lithium sheet is suitable for top-view investigation.

Electrochemical cell

A flooded two-electrode nonaqueous cell and a specially designed sample holder were used and are shown in Fig. 2, these can be easily assembled and disassembled and can avoid direct contact with the surface of the reacted lithium electrode. Our new design is especially suitable for sample transfer from the glove box for *ex situ* SEM measurements. Three types of cells were assembled with a surface flattened lithium sheet electrode. The cathode was a silicon/carbon (Si/C) composite electrode, LiCoO₂ electrode and LiFePO₄ electrode, respectively. All cathodes were composed of the active material, the conductive additive (carbon black) and the polyvinylidene fluoride (PVDF) binder at weight ratio of 92:3:5. These electrodes were prepared by spreading the active material slurry on the

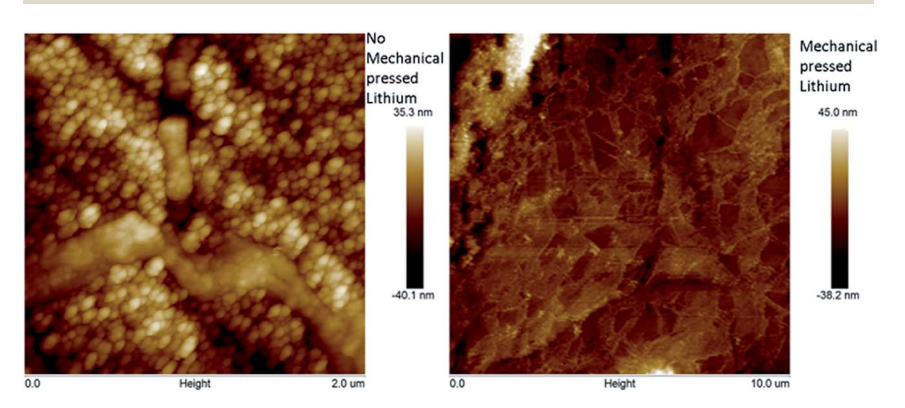


Fig. ${f 1}$ The roughness of the lithium foil before and after mechanical pressing, measured by AFM.

Table 1 Lithium roughness parameter before and after mechanical pressing

Parameter	$R_{\rm a}/{ m nm}$	$R_{ m q}/{ m nm}$	Roughness $R_{ m max}/{ m nm}$
Before press	8.02	10.0	72.7
After press	3.15	3.99	34.57

current collector (copper foils for the Si/C composites, Al foils for LiCoO₂ and LiFePO₄). Commercial electrolytes of 1 M LiPF₆ dissolved in ethylene carbonate-dimethyl carbonate (EC-DMC) (1 : 1 in v/v) without any additives were used in all cells.

Ex situ SEM investigation

As the cell was assembled, it was discharged or charged. After the discharge or charge, the cell was disassembled in the glove box and the reacted lithium foil was taken out from the cell and washed with dimethyl carbonate (DMC). The washed lithium electrode was dried in the vacuum chamber of the glove box for at least 6 hours before it was transferred to the SEM chamber of a Hitachi S4800 microscope. The special designed transfer box was used to transfer the sample, which avoid exposure of the sample to the air. In addition, a special SEM sample holder was designed to fix the installed position of the sample, which was suitable for finding the same position of the same reacted lithium electrode during each *ex situ* SEM investigation. After the SEM measurements, the lithium electrode was assembled into the cell again to be discharged or charged to next state. Such a procedure was repeated, as shown in Fig. 3.

Order of discharging and charging of lithium electrode

The Li/Si cell was discharged first. Consequently, dissolution of lithium from the lithium electrode will occur first. The Li/LiCoO₂ and Li/LiFePO₄ cell were charged first. Therefore, deposition of lithium on the counter lithium electrode will occur

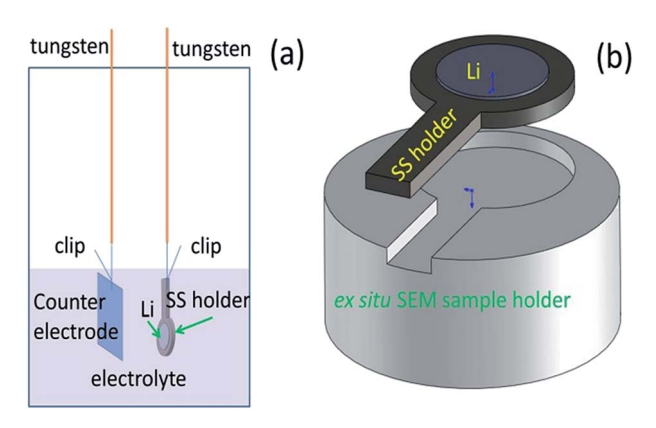


Fig. 2 Sketch of (a) a flooded two-electrode nonaqueous cell (b) sample holder for SEM investigation.

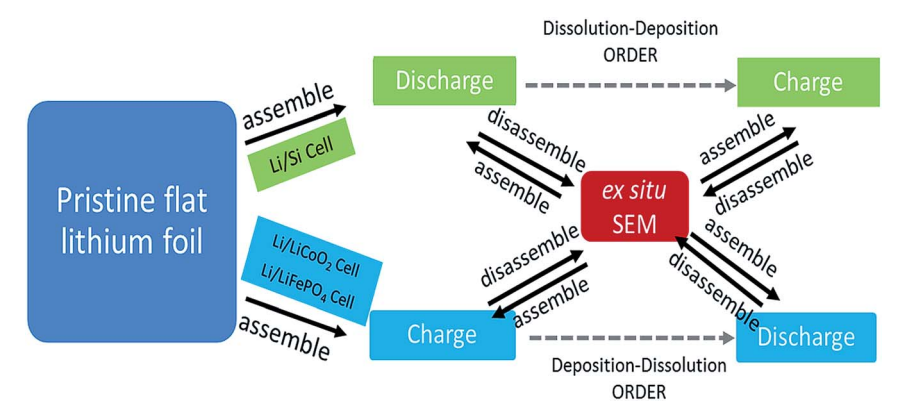


Fig. 3 The experimental design for the dissolution–deposition order and the deposition–dissolution order investigation.

first. Accordingly, we could investigate the effect of changing the discharging/charging order on the morphology change of metal lithium electrodes. The corresponding experimental details are listed in Table 2.

Second ion mass spectroscopy (SIMS) experimental

All mass spectroscopy and elemental SIMS mapping (ESM) were recorded by the Hiden SIMS Workstation to analyze the composition of the lithium electrode surface after cycling. An Ar ion gun was used. Full mass spectra were recorded using 1 nA ion current and the depth profiles were recorded using 10 nA ion current. ESM was recorded using 10 nA ion current. Two kinds of lithium foils, *i.e.* the pristine lithium foil, the lithium foil from the Li/LiFePO₄ battery at the second and 5th discharge state, were chosen for surface composition analysis. The sample transfer process was protected by a glove bag filled with argon.

In situ SEM investigation

An all-solid-state cell was used and investigated in a FEI Quanta 600 microscope, as shown in Fig. 4. The formation and growth of the lithium dendrite were investigated. In order to construct the *in situ* micro-scale all-solid-state battery setup, two tips including one Au tip and one tungsten tip were installed on the

Table 2	The cample	details of the	av citu SEM	measurements
Table /	The Samble	details of the	ex silli selvi	measurements

Cell	Charge/discharge state	Charge/discharge capacity/ mAh	SEM images	
Li/Si	Dis. to 20 mV	1.33	Fig. 6(a)	
	Dis. to 5 mV	1.47	Fig. 6(b)	
	Charge to 1 V	0.42	Fig. 6(c)	
	Dis. to 5 mV	1.40	Fig. 6(d)	
Li/LiCoO ₂	Charge to 4.2 V	3.6	Fig. 8(c) and (d)	
	Dis. to 3 V	1.78	Fig. 8(e) and (f)	
Li/LiFePO ₄	Charge to 4 V	0.26	Fig. 9(c) and (d)	
	Dis. to 2.8 V	0.15	Fig. 9(e) and (f)	

probe workstation (Kleindiek) as shown in Fig. 4. Before closing the chamber, a piece of commercial lithium foil was stuck to the tungsten tip, and the superaligned carbon nanotube (SACNT) was attached to the Au tip. The lithium metal on the tungsten tip was oxidized naturally in air before transfer to the chamber. After the chamber is closed and evacuated to about 10^{-2} Pa, the tips can be moved in three dimensions by handling the manipulator; once the SACNT on Au tip was moved to contact with the surface of the native oxide layer, the *in situ* battery was constructed. The SACNT on the Au tip, the native oxide layer Li_2O^{28} and the lithium metal on tungsten tip worked as the cathode, the solid state electrolyte and the anode, respectively. In order to induce the lithium dendrite, a bias of -3 V was applied to the SACNT ν s. Li metal.

Results and discussions

SEM image of original lithium sheet electrode

As shown in Fig. 5, it is quite clear that lithium sheet after flattening treatment does have flat surface and the defect structure is decreased, which is suitable for further SEM and AFM investigation. In this work, all lithium sheet electrodes used for AFM and SEM studies are flattened lithium sheet electrodes embedded into the SS sample holder shown in Fig. 2. For simplicity, the term "lithium electrode" will be used in later sections without extra description.

Morphology change of Li electrode in Li/Si cell

Fig. 6(a) shows a typical SEM image of the lithium electrode after the first discharge to 20 mV in the Li/Si cell. Many holes with different size and depth can be observed. In this image, the diameter of the biggest hole is about $100~\mu m$, and the depth of the hole cannot be measured. The appearance of such a large hole indicates that the electrochemical dissolution of lithium occurs more easily at the etched area. It is reasonable since the surface of the lithium electrode is covered unevenly by a layer of insulating SEI film once the lithium electrode is soaked and discharged in the electrolyte. Once the lithium electrode starts to dissolve in a certain area after discharging, some areas will be etched and the SEI surface layer covered on those areas can also be peeled off. The exposed fresh areas of the lithium electrode have a lower resistance compared to unreacted areas and are

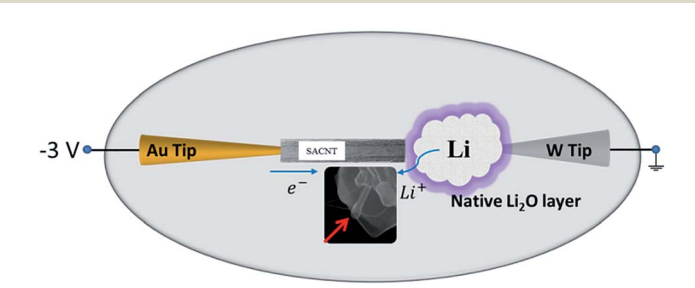


Fig. 4 The schematic illustration of the *in situ* SEM setup of all-solid-state battery. The SACNT, native Li_2O layer and Li metal worked as the cathode, solid-electrolyte and anode respectively. -3 V was applied on SACNT vs. Li metal to induce the formation of the lithium dendrite.

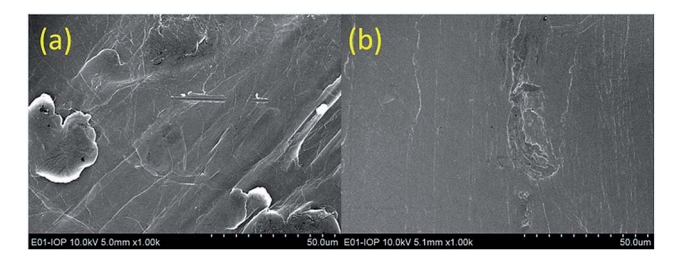


Fig. 5 (a) Original lithium foil, (b) flatten lithium foil.

can more easily be etched further. It is noted that further discharge to 5 mV seems not change too much the morphology of lithium electrode, compared to the lithium electrode discharged to 20 mV, as shown in Fig. 6(b). Some small holes can be seen clearly at the bottom inside the biggest hole and in some other regions as well.

Fig. 6(c) shows the morphology of the lithium electrode after the first charge to 1.0 V. It can be seen that the mossy-like lithium deposits back into the biggest hole of the lithium electrode which was formed mainly during discharging. We

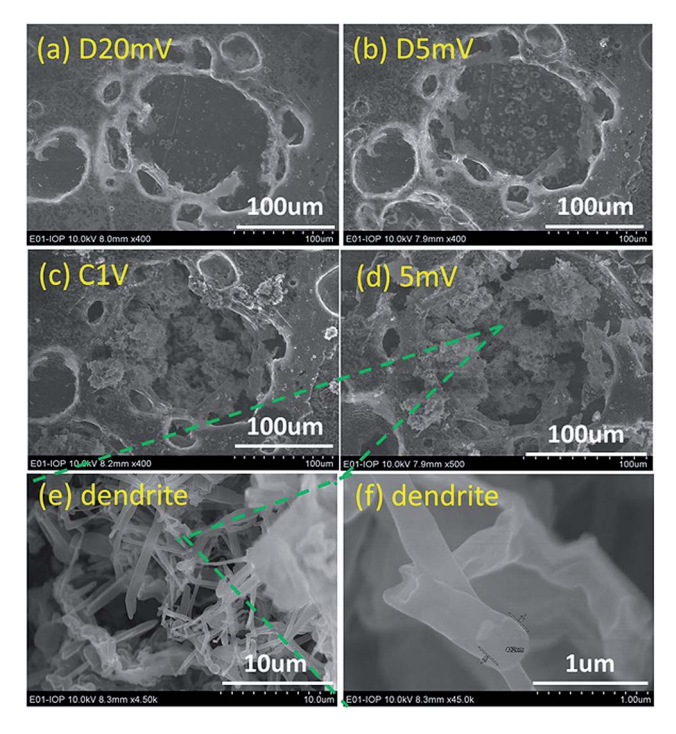


Fig. 6 Morphology evolution of the lithium electrode during lithium dissolution and deposition in the Li/Si cell. The current density for charging and discharging was 6.4 mA cm $^{-2}$. (a) 1st discharge to 20 mV; (b) 1st discharge to 5 mV; (c) 1st charge to 1 V; (d) 2nd discharge to 5 mV; (e and f) SEM images of the dendrite-like lithium which deposited in the hole.

did not observe that lithium is deposited on the flat surface of the lithium electrode during charging. This indicates that once the holes are formed, that area becomes more electrochemically active than the unreacted flattened areas.

Fig. 6(d) shows the morphology of the lithium electrode after the second discharge to 5 mV. The morphology does not change too much and the filled mossy-like lithium in the big hole still exists but the amount decreases. The edge part of the big hole is destroyed slightly. At high magnification in Fig. 6(e) and (f), it can be observed clearly that the mossy-like lithium has the dendrite appearance. The diameter is about 400 nm in this case.

To get a whole impression, low resolution images of the lithium electrode in the Li/Si cell at different states are shown in Fig. 7. In the center area of the lithium electrode, many holes can be seen clearly after the first discharge to 20 mV. The distribution of the holes is random. The hole size is about 50–100 μm . The density and size of the holes increases after further discharging to 5 mV. Some holes have merged together. At the edge part, it is noted that dendrite-like lithium is observed, as shown in Fig. 7b and c. After the second discharge, the surface becomes significantly rougher. From Fig. 7d, it is quite obvious, that the many deposited mossy-like lithium structures still remain on the surface of the lithium electrode; it is quite plausible that the remaining deposited lithium after the second discharge becomes "dead" lithium.

The morphology evolution of the lithium electrode in the Li/LiCoO_2 cell is shown in Fig. 8. The pristine lithium electrode has a flat surface and is free of any deposited lithium.

In the charged state, the surface of the lithium electrode is covered by granular species, as shown in Fig. 8c and d. The distribution of the granules can be regarded as random, although parallel stripes can be seen. At the discharge state, most of the granular species remain. Note that the coulombic efficiency of the Li/LiCoO₂ cell is 49% (calculated from the Table 2, 1.78/3.6 = 49%), which means that only 49% deposited lithium dissolves from the lithium electrode during

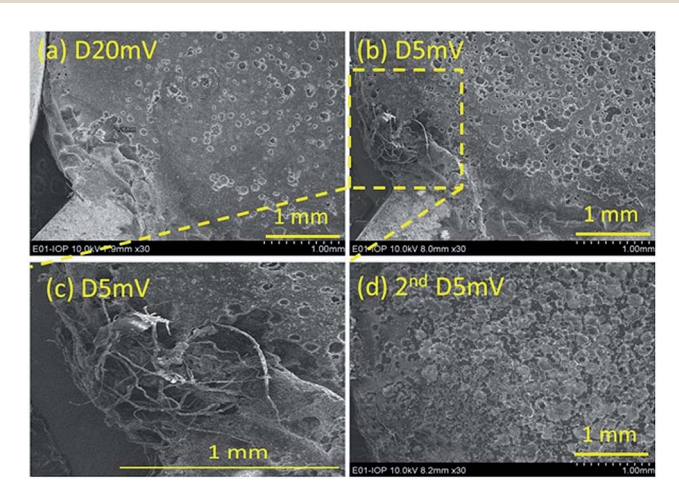


Fig. 7 Evolution of lithium electrode in Li/Si system at different states: (a) 1st discharge to 20 mV; (b) 1st discharge to 5 mV; (c) 1st discharge to 5 mV, edge part; (d) 2nd discharge to 5 mV.

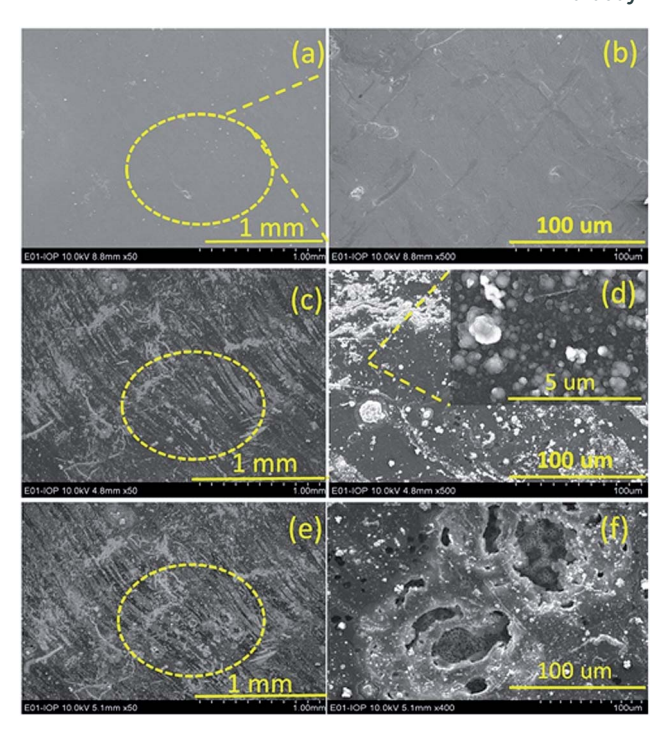


Fig. 8 Morphology evolution of the lithium electrode during lithium dissolution and deposition in the Li/LiCoO₂ cell. The current density for charging and discharging was 6.4 mA cm⁻². (a) pristine lithium; (b) zoomed image of the marked area of pristine lithium; (c) 1st charge to 4.2 V; (d) zoomed image of the marked area in the image (c); (e) 1st discharge to 3 V; (f) zoomed image of the marked area in the image (e).

discharging. This calculation is consistent with the phenomena that the granular species still remain after discharge. It is also noted that many holes appear, like in Fig. 6 and 7. This indicates further that the hole structure is more electrochemically active than the flat surface and deposited granular lithium on the surface of the lithium electrode.

In both cases of Li/Si cell and Li/LiCoO₂ cell, the current density during discharging and charging was 6.4 mA cm⁻² and the corresponding capacity for the dissolution and deposition of lithium is about 1–3 mA h. Such capacity and current density are comparable values for the discharging and charging of commercial lithium batteries. In order to study the effect of the current density and capacity on the morphology of the lithium electrode, another Li/LiFePO₄ cell was tested with one tenth of the current density and the capacity of the Li/LiCoO₂ cell. As shown in Fig. 9c, a few granular particles can be seen on the surface of the lithium electrode after charging. After discharging many holes with a size of 10 µm appeared, accompanied with some smaller holes. These phenomena are similar to the case of Li/LiCoO₂ cell, but quite possibly in the early stages.

Since the lithium electrode has excellent electronic conductivity and ionic conductivity, the electrolyte has also high ionic conductivity and high concentration, therefore, it is not likely that the inhomogeneity of the transport of electron and lithium cations in the lithium electrode and inhomogeneous ionic

flow leads to the formation of an inhomogeneous hole structure and dendrite/granular/mossy-like lithium. We suspect that the SEI on the lithium electrode plays a key role to influence the morphology of the lithium electrode during electrochemical dissolution and deposition in nonaqueous lithium cells. However, it is not very easy to detect the homogeneity of the SEI on the lithium electrode. We performed SIMS to investigate this issue indirectly.

SIMS investigation on surface compositions

With the sample holder, it is convenient to scan the negative ion full mass spectrum of the pristine and reacted lithium electrode by the SIMS technique. The lithium electrode after five cycles in a Li/LiFePO₄ cell is detected and the full negative ion mass spectrum is shown in Fig. 10.

According to the negative ion spectroscopy, the four elements (namely H, C, O, F) on the surface can be identified. Li, C and N can be identified from the positive ion spectrum. Accordingly, the SIMS results are consistent with previous investigations, which demonstrated that the SEI on the surface of lithium electrode contains Li₂CO₃, LiF, Li₂O.²⁹⁻³¹

With the cycling scanning, the depth distribution of every element can be also detected. The scanning mode using a small ion beam current (1 nA) and in spot

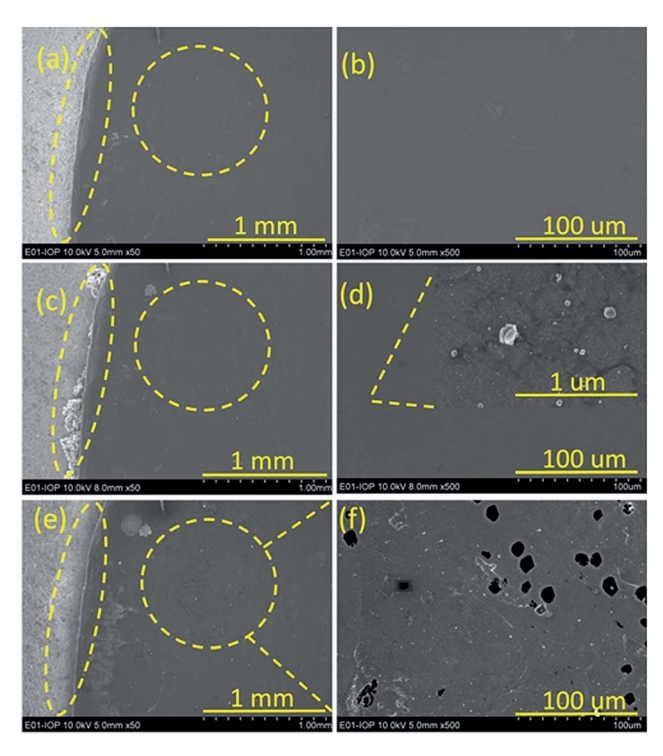


Fig. 9 Morphology evolution of the lithium electrode during lithium dissolution and deposition in the Li/LiFePO₄ cell. Current density for charging and discharging was 0.64 mA cm⁻². (a) Pristine; (b) zoomed image in marked circle area in image (a); (c) charge to 4 V; (d) zoomed image of the marked area in the image (c); (e) discharge to 2.8 V; (f) zoomed image of the marked area in the image (e).

mode can only get depth information from the surface of the sample. In this work, a raster mode provided by the Hiden SIMS was used, which applied a bigger ion beam current (100 nA) and can reflect the depth profile more accurately. Fig. 11 shows the SIMS signals from the strongest two peaks of F and O. It can be seen that concentration of fluorine on the surface is increased significantly after cycling and the concentration of oxygen decreases. This is reasonable, as LiF covers gradually the pristine oxide layer.

Elemental SIMS mapping was also performed and is shown in Fig. 12. The element distribution on the surface of the lithium electrode is inhomogeneous. The element mapping consists of the depth profiles: the concentration of fluorine is increased and the oxygen is decreased after cycling. Accordingly, the coverage of the SEI on the lithium electrode is inhomogeneous and the outer layer is enriched with fluorine.

In situ SEM investigation on the growth of lithium dendrite

Furthermore, lithium dendrite formation was investigated by the means of *in situ* SEM. Currently, we cannot perform *in situ* SEM investigation on a liquid nonaqueous cell. We built an all-solid-state battery in the SEM chamber (see Fig. 4), with the SACNT, the native oxide layer on lithium surface, the Li metal as the cathode, solid-electrolyte and anode, respectively.³² As shown in Fig. 13, –3 V was applied to the SACNT vs. Li metal, to discharge the all-solid-state battery. It is observed that the lithium dendrite is formed after applying an external electrical field for 700 s (Fig. 13b), and it grew along a random direction until it overlapped the SACNT (Fig. 13a–c). Once the dendrite and SACNT overlapped each other, the dendrite started to grow along the SACNT, rather than along the previous growth direction. The growth of the lithium dendrite has to be accompanied with the transportation of lithium ions and electrons, which may be due to the high electronic conductivity of CNT. This phenomenon means that after growing to a certain length, the electron flow could also guide the formation of lithium dendrite.

Actually, the whole process of the dendrite growth was followed and captured; Fig. 13(a)–(d) were just selected for demonstration. In addition, the size evolution of the dendrite was extracted from the *in situ* captured images, as plotted in

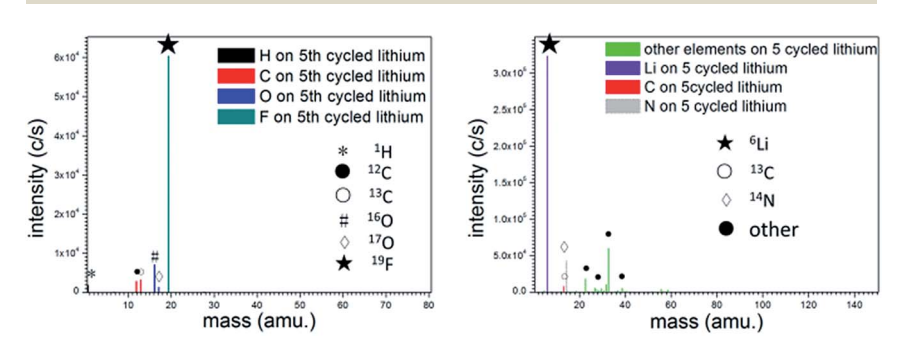


Fig. 10 SIMS full negative ion mass scanning spectrum (left) and positive ion spectrum (right) of the lithium electrode after 5 cycles. The current density was 0.64 mA cm^{-2} .

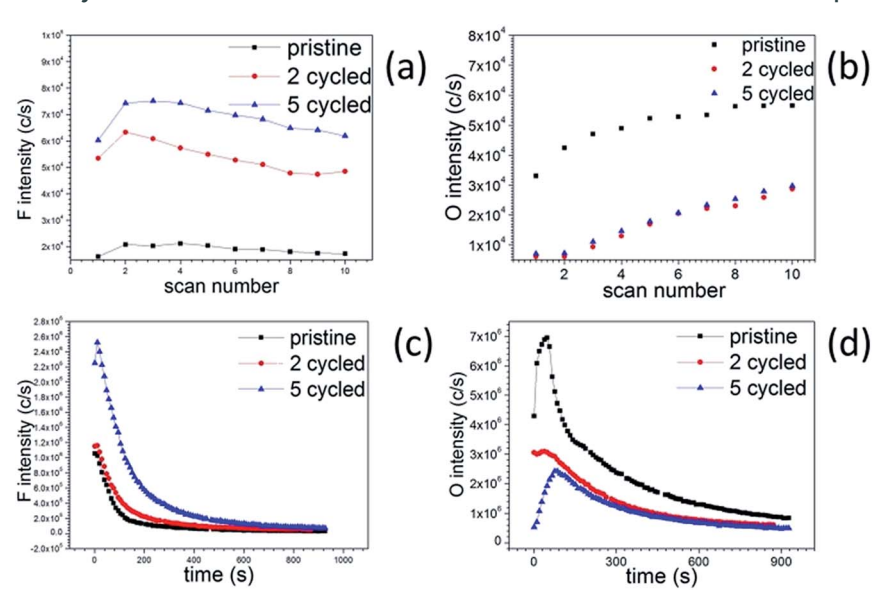


Fig. 11 The surface depth distribution of (a) fluorine and (b) oxygen, and the element depth profile of (c) fluorine and (d) oxygen in a pristine lithium electrode, after the second cycle, and the fifth cycle.

Fig. 13(e). It is demonstrated that the growth of the dendrite was a diffusion-controlled process.

The formation of the dendrite lithium in the *in situ* SEM experiment means that the lithium ions can migrate across the surface $\mathrm{Li_2O}$ layer, nucleate on the top of the $\mathrm{Li_2O}$ covered lithium electrode and grow into the dendrite. These results are consistent with the appearance of the lithium dendrite of the Li/Si cell during discharging (lithium extraction) shown in Fig. 7(c). It is also interesting to notice that as the diameter of the lithium dendrite remains the same (about 470 nm), the length of the dendrite increases continuously to as long as 1.72 μ m (Fig. 13(d)). Further finite element simulation is being carried out.

As investigated above, in both *ex situ* SEM and *in situ* SEM, the formation of dendrite-like lithium can occur in both dissolution and deposition. In the case of dissolving first, large holes are formed randomly after delithiation and dendrite-like and mossy-like lithium preferentially fill the holes after lithiation. In the case of depositing first, granular-like lithium will deposit on the surface of the lithium electrode randomly after lithiation. The hole-like structure forms again on the surface in spite of covered by granular-like lithium. Since the surface of lithium electrode is covered unevenly by a layer of SEI, the dissolution and deposition of lithium are not uniform. Whatever the charging/discharging (dissolution–deposition) order, mossy-like or granular-like lithium cannot disappear. These phenomena will definitely lead to the formation of "dead" lithium, which is not favorable for achieving good cyclic performance and high coulombic efficiency for rechargeable lithium batteries.

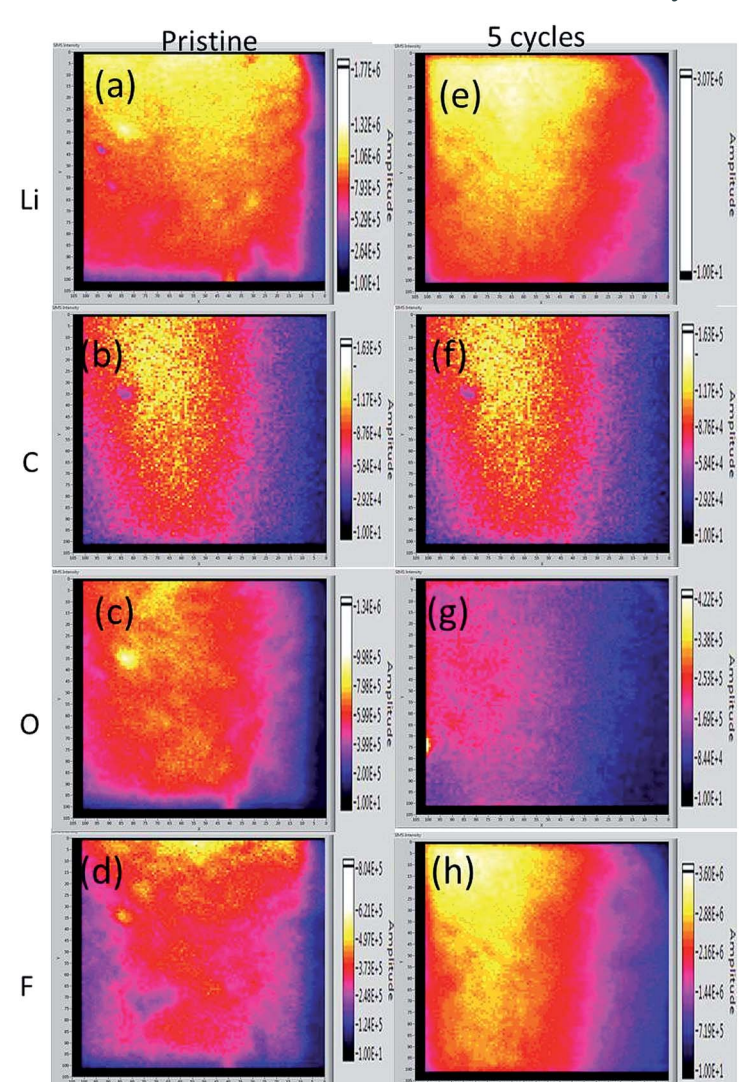


Fig. 12 ESM of Li,F, C, O: (a), (c), (e) and (g) in the pristine lithium and (b), (d), (f) and (h) in the 5-cycle lithium electrode.

Our report shows that top-view direct observation of the morphology of the lithium electrode is now technologically feasible. Combining with AFM, conducting AFM, XPS and SIMS, it is possible to understand clearly the evolution of the structure and chemical composition of the lithium electrode in rechargeable lithium batteries. Further investigations on the morphology of the lithium electrode in different lithium batteries, nonaqueous electrolytes with functional additives, surface coatings with solid electrolytes and different atmospheres are being carried out. Those investigations should be essential for developing rechargeable lithium batteries.

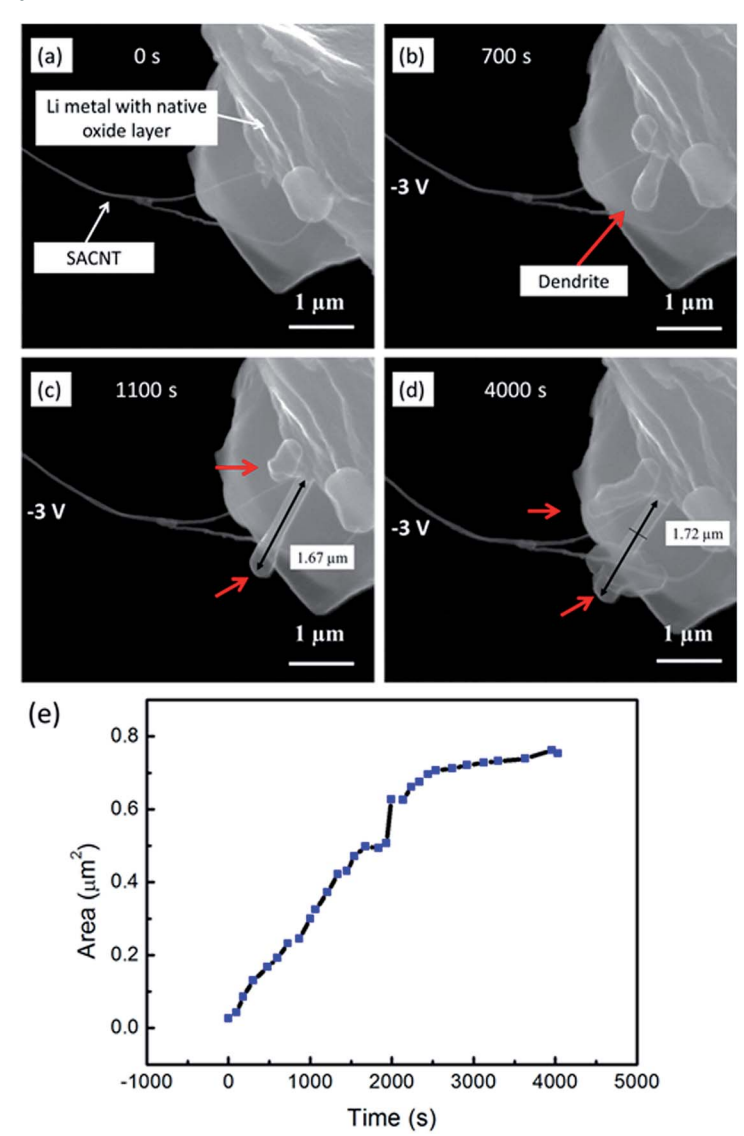


Fig. 13 The morphology evolution of the lithium dendrite in an *in situ* all-solid-state battery; the lithium dendrites were indicated by red arrows. (a–d) show the selected morphology of the lithium dendrite, with the electrical field applied for 0 s, 700 s, 1000 s, 4000 s respectively. The increase of the cross sectional area of the lithium dendrite is plotted in (e).

Conclusions

A flat surface of lithium electrode with a hard stainless steel sample holder is designed for $ex\ situ\ SEM$ investigation. In the case of the Li/Si cell, a large amount of hole-like structures with 100 μm hole size and a small amount of lithium dendrites have been observed after discharging. Mossy-like and dendrite-like

lithium are found mainly in the holes formed during discharging. Some of them do not disappear after the second discharge, indicating the existence of "dead lithium". In the case of Li/LiCoO₂ and Li/LiFePO₄ cells, granular like lithium is found on the surface of the lithium electrode after the first charging. Quite a lot of granular-like lithium remains after the first discharging. In addition, hole-like structures appear again. *In situ* SEM demonstrates clearly that the lithium dendrite could grow on the surface oxide (Li₂O) covered lithium during discharging of the Li/Li₂O/SACNT cell. Inhomogeneous deposition and dissolution of dendrite/mossy/granular like lithium and hole-like structures is believed to be related to inhomogeneous coverage of the SEI film, not likely to be related to the homogeneity of the electronic or ionic conductivity of the lithium electrode.

Acknowledgements

Financial supports from the NSFC project (51325206), Beijing S&T Project (Z13111000340000), and "Strategic Priority Research Program" of the Chinese Academy of Sciences, Grant no. (XDA0901010000) are appreciated. We thank Prof. Kaili Jiang's group from Tsinghua University, they provided very nice SACNTs in the *in situ* SEM experiment.

Notes and references

- 1 C. X. Zu and H. Li, *Energy Environ. Sci.*, 2011, **4**, 2614; J. Y. Peng, C. X. Zu and H. Li, *Energy Storage Sci. Technol.*, 2013, **2**, 55.
- 2 M. Winter, J. O. Besenhard, M. E. Spahr and P. Novak, Adv. Mater., 1998, 10, 725
- 3 J. M. Tarascon and M. Armand, Nature, 2001, 414, 359.
- 4 J. B. Goodenough and Y. Kim, Chem. Mater., 2010, 22, 587.
- 5 B. Scrosati and J. Garche, J. Power Sources, 2010, 195, 2419.
- 6 B. Dunn, H. Kamath and J. M. Tarascon, Science, 2011, 334, 928.
- 7 D. Aurbach, Nonoaqueous Electrochemistry, Marcel Dekker, New York, 1999.
- 8 H. Kim, G. Jeong, Y. U. Kim, C. J. H. Kim, C. M. Park and H. J. Sohn, *Chem. Soc. Rev.*, 2013, **42**, 9011.
- 9 K. Xu, Chem. Rev., 2004, 104, 4303.
- 10 Z. I. Takehara and K. I. Kanamura, Electrochim. Acta, 1993, 38, 1169.
- 11 D. Aurbach, B. Markovsky, A. Shechter and Y. Ein-E1i, *J. Electrochem. Soc.*, 1996, **143**, 3809.
- 12 S. Shiraishi, K. Kanamura and Z. Takehara, Langmuir, 1997, 13, 3542.
- 13 F. Orsini, A. Du Pasquier, B. Beaudoin, J. M. Tarascon, M. Trentin, N. Langenhuizen, E. De Beer and P. Notten, *J. Power Sources*, 1998, **76**, 19–29.
- 14 C. Brissot, M. Rosso, J. N. Chazalviel and S. Lascaud, J. Power Sources, 1999, 81–82, 925.
- 15 M. Dollé, L. Sannier, B. Beaudoin, M. Trentin and J. M. Tarascon, *Electrochem. Solid-State Lett.*, 2002, 5, A286.
- 16 D. Aurbach, B. Markovsky, M. D. Levi, E. Levi, A. Schechter, M. Moshkovich and Y. Cohen, J. Power Sources, 1999, 81–82, 95.
- 17 K. Morigaki, J. Power Sources, 2002, 104, 13.
- 18 W. S. Kim and W. Y. Yoon, Electrochim. Acta, 2004, 50, 541.

- 19 S. Chandrashekar, N. M. Trease, H. J. Chang, L.-S. Du, C. P. Grey and A. Jerschow, *Nat. Mater.*, 2012, 11, 311.
- 20 R. Bhattacharyya, B. Key, H. Chen, A. S. Best, A. F. Hollenkamp and C. P. Grey, Nat. Mater., 2010, 9, 504.
- 21 D. Aurbach, Y. Ein-Eli and A. Zaban, J. Electrochem. Soc., 1994, 141, L1.
- 22 D. Aurbach, M. L. Daroux, P. W. Faguy and E. Yeager, *J. Electrochem. Soc.*, 1988, 135, 1863.
- 23 K. Kanamura, S. Shiraishi and Z.-I. Takehara, *J. Electrochem. Soc.*, 1994, 141, L108.
- 24 D. Aurbach, I. Weissman, A. Schechter and H. Cohen, *Langmuir*, 1996, 12, 3991.
- 25 M. Odziemkowski, M. Krell and D. E. Irish, J. Electrochem. Soc., 1992, 139, 3052.
- 26 P. C. Howlett, D. R. MacFarlane and A. F. Hollenkamp, J. Power Sources, 2003, 114, 277.
- 27 J. Y. Zheng, H. Zheng, R. Wang, L. B. Ben, W. Lu, L. W. Chen, L. Q. Chen and H. Li, *Phys. Chem. Chem. Phys.*, 2014, **16**, 13229.
- 28 X. H. Liu and J. Y. Huang, Energy Environ. Sci., 2011, 4, 3844.
- 29 J. B. Bates, US Pat., 5,314,765, 1994, pp. 5-24.
- 30 X. Wang, Y. Hou, Y. Zhu, Y. Wu and R. Holze, Sci. Rep., 2013, 3, 1401.
- 31 S. H. Lee, J. R. Harding, D. S. Liu, J. M. D'Arcy, Y. Shao-Horn and P. T. Hammond, *Chem. Mater.*, 2014, 26, 2579–2585.
- 32 N. Choi, Solid State Ionics, 2004, 172, 19-24.